Electrothermal Simulation and Optimal Design of Thermoelectric Cooler Using Analytical Approach

Liang Chen[®], Member, IEEE, Sheriff Sadiqbatcha[®], Graduate Student Member, IEEE, Hussam Amrouch[®], Member, IEEE, and Sheldon X.-D. Tan[®], Senior Member, IEEE

Abstract—In this article, electrothermal modeling and simulation of thermoelectric cooling (TEC) in the package design of VLSI systems are performed by solving coupled heat conduction and current continuity equations. We propose a new analytical solution to the coupled partial differential equations (PDEs) which describe temperature and voltage with the reduction from 3-D to 1-D. In addition to this, we derive new analytic expressions for two key performance metrics for TEC devices: 1) the maximum temperature difference and 2) the maximum heatflux pumping capability, which can be guided for the optimal design of thermoelectric cooler to achieve the maximum cooling performance. Furthermore, for the first time, we observe that when the dimensionless figure of merit ZT_0 value is larger than 1, there is no maximum heat-flux value, which means the heat dissipation due to the Peltier and Fourier transfer effects is larger than the heat generation caused by the Joule heating effect, which can lead to more efficient TEC cooling design. The accuracy of the proposed 1-D formulas is verified by a 3-D finite element method using COMSOL software. The compact model delivers many orders of magnitude speedup and memory saving compared to COMSOL with marginal accuracy loss. Compared with the conventional simplified 1-D energy equilibrium model, the proposed analytical coupled multiphysics model is more robust and accurate.

Index Terms—Analytical solution, electrothermal simulation, figure of merit, thermoelectric cooler.

I. Introduction

THERMOELECTRIC cooler (TEC) has become the most promising active cooling technique for thermal management in VLSI chips, electronic devices, and semiconductor lasers because of its light weight, precise control, high reliability, and noiseless operation [1]–[11]. With the Peltier effect driven by the electric current, the TEC transfers heat from one side to the other.

Manuscript received 4 November 2020; revised 27 April 2021 and 30 September 2021; accepted 10 October 2021. Date of publication 15 October 2021; date of current version 22 August 2022. This work was supported in part by NSF under Grant CCF-1527324, Grant CCF-1816361, Grant CCF-2113928, and Grant OISE-1854276. This article was recommended by Associate Editor E. R. Keiter. (Corresponding author: Sheldon X.-D. Tan.)

Liang Chen, Sheriff Sadiqbatcha, and Sheldon X.-D. Tan are with the Department of Electrical and Computer Engineering, University of California at Riverside, Riverside, CA 92521 USA (e-mail: stan@ece.ucr.edu).

Hussam Amrouch is with the Chair for Semiconductor Test and Reliability, The University of Stuttgart, 70569 Stuttgart, Germany (e-mail: amrouch@iti.uni-stuttgart.de).

Digital Object Identifier 10.1109/TCAD.2021.3120533

Temperature distribution of microprocessors is nonuniform and there are localized hot spots with different sizes and power densities, which are located at different positions. Fortunately, the advantage of using TEC is the ability to directly provide localized cooling at small regions with high power densities and consequently achieve high cooling efficiency [1], [4]–[7], [10]. Recently, many research works have been carried out to improve the cooling heat flux values of TEC [1]–[3], [12]–[15]. On the other hand, an accurate TEC model and its corresponding fast analysis are significant for optimizing the TEC design to reach the best cooling performance.

A simplified 1-D energy equilibrium model was first proposed to characterize the cooling heat flux of the TEC device based on energy balance on the cold side [1], [3], [16], [17]. However, this model is an approximated expression, which is overly simplified. Consequently, the simplified 1-D model fails to provide accurate results when the thermal gradient is large.

To model TEC devices accurately, the 3-D coupled multiphysics model was developed based on the coupled heat conduction equation and current continuity equation [3], [18]–[20]. Therefore, numerous efforts on solving the partial differential equations (PDEs) describing thermal and electric fields have been made to perform multiphysics simulation of the TEC [8], [18], [21]-[25]. There are several numerical methods for solving PDEs, such as the finiteelement method [18], [21], finite-difference method [25], and finite-volume method [22]–[24]. However, the numerical methods are very time consuming due to the need of parameter tuning and optimization for the design of the TEC. To improve the efficiency, an analytical approach, called the separation of variables method, was proposed to describe transient and steady thermal behavior of the TEC based on 1-D thermal path modeling [8]. Such a closed-form solution can provide better insights into TEC-based cooling. The work in [8], however, ignored the coupling effects between thermal and electric fields, and also did not obtain the maximum cooling heat flux values, which is a key parameter of the TEC device.

In this work, we develop a new analytical solution to perform the coupled electrothermal co-simulation and optimization for the TEC device. Our novel contributions are as follows.

1937-4151 © 2021 IEEE. Personal use is permitted, but republication/redistribution requires IEEE permission. See https://www.ieee.org/publications/rights/index.html for more information.

- We propose a new analytical solution to the coupled heat conduction and current continuity equations describing thermal and electric fields.
- 2) Based on the closed-form exact solution, we derive two important performance metrics for TEC devices: a) the maximum temperature difference $\Delta T_{\rm max}$ with heat flux q=0 and b) the maximum cooling heat flux $q_{\rm max}$ with $\Delta T=0$.
- 3) Based on the closed-form analytic expressions describing the relationship between the cooling heat flux and voltage, for the first time, we observe that when the dimensionless figure of merit ZT_0 value is larger than 1, the cooling heat-flux value increases with the increasing voltage. This is because the heat dissipation due to Peltier and Fourier transfer effects is larger than the heat generation caused by the Joule heating effect. This configuration can lead to a more efficient TEC cooling design. Furthermore, we observe that increasing ZT_0 of TEC and decreasing TEC thickness L can improve the maximum cooling heat flux $q_{\rm max}$.
- 4) Finally, the accuracy of the proposed analytical method is validated by the finite-element-based COMSOL mathematics module. Numerical results on the TEC leg with different parameters, such as Seebeck coefficient S, thermal conductivity κ , electrical conductivity σ , constant temperature T_0 , and length L show that the proposed method has a good agreement with COMSOL. The compact model delivers many orders of magnitude speedup and memory saving compared to COMSOL with marginal accuracy loss. Compared with the conventional simplified 1-D energy equilibrium model, the proposed analytical coupled multiphysics model is more robust and accurate.

The remainder of this article is organized as follows. Section II reviews the simplified 1-D energy equilibrium model and 3-D coupled multiphysics model. Section III derives an analytical solution for the 3-D coupled multiphysics model with the reduction from 3-D to 1-D. Section IV obtains the maximum temperature difference and cooling heat flux of TEC based on the analytical expression. Section V shows numerical results and their comparison of the proposed method, the commercial software COMSOL and the simplified 1-D energy equilibrium model. Section VI concludes this article.

II. REVIEW OF RELEVANT WORK

In chip package, thin-film TEC devices are immersed in the thermal interface materials (TIMs) layer to remove the heat generated by VLSI chips, as shown in Fig. 1(a). With high thermal conductivity, heat spreader transfers the heat to heat sink homogeneously. Based on air convection cooling, heat sink can dissipate the heat efficiently. Fig. 1(b) shows a detailed 3-D view of the thin-film TEC devices, which consist of N-type and P-type materials. These N-P pairs of legs are connected in series with the two *hot* side terminals connected together, and the two *cold* side terminals connected to the opposite ends of a battery as shown in Fig. 1(c). When

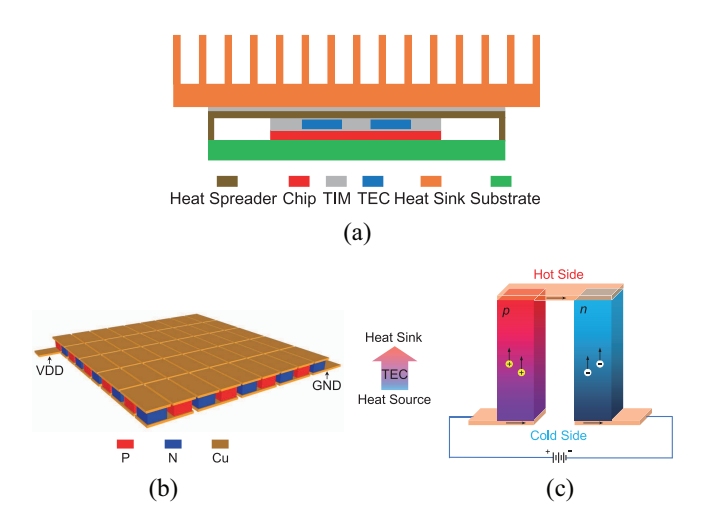


Fig. 1. (a) Side view of the chip package. (b) 3-D view of thin-film TEC devices. (c) Peltier effect for an N-P pair in the TEC devices.

the current flows from the cold side to the hot side, heat is absorbed from heat sources located at the cold (bottom) side and generated on the hot (top) side with the heat sink.

We remark that the TEC device is set up so that it moves heat from chip side to the ambient (or heat sink) side regardless of the real temperature difference between the chip side and the ambient side. The *cold* and *hot* notations in TEC mean heat flow such that the TEC device absorbs heat at the *cold* side and generates heat at the *hot* side. The actual temperature difference of the two sides can be any value.

A. Thermoelectric Effects in Nutshell

The TEC devices remove heat from the chip efficiently based on the thermoelectric (TE) effect. The TE effect, which is an energy conversion between electric and thermal fields, consists of five different physics: 1) Seebeck; 2) Peltier; 3) Thomson; 4) Joule heating; and 5) Fourier transfer effects.

We note that the Seebeck effect represents that temperature difference can lead to voltage difference, which is represented by the equation $\nabla V = S \nabla T$, where V is the voltage, T is the temperature, S is the Seebeck coefficient (V/K), and ∇ is the vector gradient operator [16]. We assume that the two ends of the TE material are excited by an ideal voltage source, which is capable of supplying and maintaining the same voltage. Under these conditions, the voltage remains a constant value although the working load changes with the temperature difference. In other words, the Seebeck effect will not come into play in this setting. Therefore, with the assumption of an ideal voltage source, we do not consider the Seebeck effect. The Thomson effect is typically ignored for the constant Seeback coefficient. In the following, we briefly review Peltier, Fourier transfer, and Joule heating effects.

First, under the Peltier effect, the current density \mathbf{J} (A/m²), driven by the voltage across two ends, produces heat flux \mathbf{q}_P moving from cold side to hot side, which is expressed as [16]

$$\mathbf{q}_{\mathbf{P}} = P\mathbf{J} \tag{1}$$

where $P = S \times T$ is the Peltier coefficient, and heat flux \mathbf{q}_P is a flow of heat energy per unit area per unit time (W/m²).

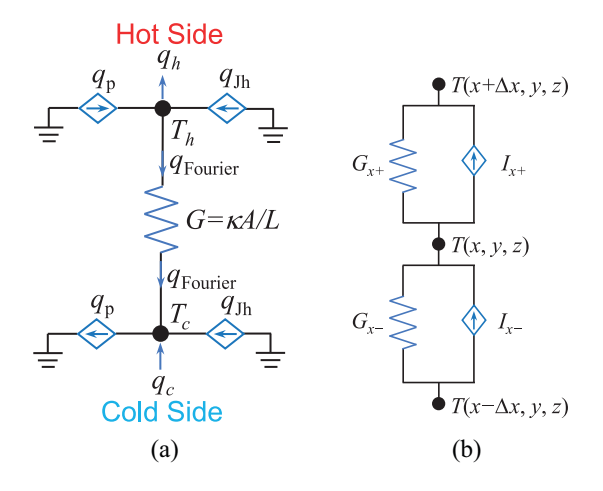


Fig. 2. Equivalent thermal circuits of a TEC leg based on (a) simplified 1-D energy equilibrium model and (b) 1-D reduction of 3-D coupled multiphysics model.

Second, Fourier's law describes that the heat flux flows from high temperature to low temperature, which is expressed as

$$\mathbf{q}_{\text{Fourier}} = -\kappa \nabla T \tag{2}$$

where κ is the thermal conductivity.

Last, the power per unit volume (W/m³) due to the Joule heating effect is calculated by

$$g_{Jh} = \mathbf{J} \cdot \mathbf{E} = \frac{||\mathbf{J}||^2}{\sigma} \tag{3}$$

where σ is the electrical conductivity, **E** is the electric field, "·" is the dot product operator, $||\mathbf{J}||^2$ is the dot product of **J** and itself, and **J** is equal to the product of σ and **E**. To model the TE effect, two models were primarily investigated in the existing work [3], [16], [18]. One is a simplified 1-D energy equilibrium model and the other is a more complicated 3-D coupled multiphysics model. We briefly review both in the following section.

B. Simplified 1-D Energy Equilibrium Model

In this section, we first review the existing work for 1-D TEC device modeling and related important results. A simplified 1-D energy equilibrium model was first proposed to characterize the cooling heat flux of the TEC device based on energy balance on the cold side. We assume that the 1-D represents *x*-direction.

Fig. 2(a) shows that the simplified 1-D energy equilibrium model can be represented by an equivalent thermal circuit [5]–[7], [26]. On the cold side, based on Kirchoff's current law, the cooling heat flux, which is a key parameter to represent the cooling capacity of TEC, is calculated by [1], [3], and [16]

$$q_c = q_{\rm P} - q_{\rm Jh} - q_{\rm Fourier} \tag{4}$$

where T_c and T_h are the temperatures on the cold and hot sides, respectively, J is current density along the positive direction of x-axis (J > 0), and L is the thickness of the TEC leg. The heat flux due to Fourier transfer effect is expressed as

$$q_{\text{Fourier}} = -\kappa \nabla T \approx -\kappa \frac{\Delta T}{\Delta x} = \kappa \frac{T_h - T_c}{L}.$$
 (5)

As shown in Fig. 2(a), we can use thermal conductance G to describe Fourier's law. The value of thermal conductance is calculated by

$$G = \kappa \frac{A}{L} \tag{6}$$

where A is the cross sectional area of the TEC leg. The effective heat flux caused by Joule heating on the cold side is calculated by

$$q_{\rm Jh} \approx \frac{1}{2} \frac{Q_{\rm Jh}}{A} = \frac{1}{2} \frac{g_{\rm Jh} \mathcal{V}}{A} = \frac{1}{2} \frac{J^2 L}{\sigma} \tag{7}$$

where V is the volume of the TEC leg, g_{Jh} is defined in (3), and Q_{Jh} is the heat produced by Joule heating. The formulas on the hot side are similar to (8) of the cold side [16]. Based on (1), (4), (5), and (7), the cooling heat flux is represented by

$$q_c = ST_c J - \frac{1}{2} \frac{J^2 L}{\sigma} - \frac{\kappa}{L} (T_h - T_c).$$
 (8)

There are two key TEC performance metrics—maximum cooling heat flux and maximum temperature difference. In general, each TEC vendor provides these parameters for their TEC devices. The approximated expression (8) is employed to calculate the two important parameters to estimate the TEC's performance [16], [17].

Specifically, temperature difference ΔT between the hot and cold sides is defined at zero heatload; which means the cold side is adiabatic ($q_c = 0$). With $q_c = 0$, we have

$$q_c = ST_c J - \frac{1}{2} \frac{J^2 L}{\sigma} - \frac{\kappa}{L} (T_h - T_c) = 0.$$
 (9)

Based on (9), we obtain the temperature on the cold side

$$T_c = \frac{T_h + 0.5 \frac{J^2 L^2}{\kappa \sigma}}{1 + \frac{SJL}{\kappa}}.$$
 (10)

Generally, the heat sink is placed on the hot side so that the heat can be pumped quickly from the heat source to heat sink. Therefore, temperature T_h on the hot side is considered to be a constant value T_0 . Therefore, the temperature difference is expressed as

$$\Delta T = T_h - T_c = T_0 - \frac{T_0 + 0.5 \frac{J^2 L^2}{\kappa \sigma}}{1 + \frac{SJL}{\kappa}}.$$
 (11)

To obtain the maximum value of ΔT , the derivative of (11) is set to 0, which leads to

$$\frac{\partial \Delta T}{\partial J} = -\frac{\frac{JL^2}{\kappa \sigma} \left(1 + 0.5 \frac{SJL}{\kappa} \right) - \frac{SLT_0}{\kappa}}{\left(1 + \frac{SJL}{\kappa} \right)^2} = 0. \tag{12}$$

Then, we obtain the optimal current density for generating the maximum temperature difference

$$J_{\text{opt},T} = \frac{\kappa}{LS} \left(-1 + \sqrt{1 + 2ZT_0} \right) \tag{13}$$

where Z is the material's figure of merit [16]

$$Z = \frac{S^2 \sigma}{r} \tag{14}$$

which depends on the parameters of thermoelectric materials. Based on Ohm's law $J = \sigma(V/L)$, the optimal voltage is given by

$$V_{\text{opt},T} = \frac{\kappa}{S\sigma} (-1 + \sqrt{1 + 2ZT_0}).$$
 (15)

Therefore, the resulting maximum temperature difference is written as

$$\Delta T_{\text{max}} = T_0 - \frac{\sqrt{1 + 2ZT_0} - 1}{Z}.$$
 (16)

 $\Delta T_{\rm max}$ is the maximum possible temperature difference that TE devices can create between the two sides without heat source (such as chip die). This important parameter is determined by the material's figure of merit Z and the temperature on the hot side T_0 . Therefore, ZT_0 is actually defined as a dimensionless figure of merit [16]. Hence, the increasing ZT_0 can improve the maximum temperature difference $\Delta T_{\rm max}$. Note that the thickness L of TEC has no impact on the maximum temperature difference.

Now let us look at the cooling heat flux q_c on the cold side, which is defined with zero temperature difference ($\Delta T = 0$). Based on $T_h = T_c = T_0$, we obtain

$$q_c = ST_0 J - \frac{1}{2} \frac{J^2 L}{\sigma}.$$
 (17)

Similarly, with the derivative $[\partial q_c/\partial J] = 0$, we obtain the optimal current density and voltage to reach the maximum cooling heat flux as shown in the following:

$$J_{\text{opt},q} = \frac{S\sigma T_0}{I} \text{ and } V_{\text{opt},q} = ST_0.$$
 (18)

The corresponding maximum cooling heat flux is given by

$$q_{\text{max}} = 0.5 \frac{S^2 T_0^2 \sigma}{L}.$$
 (19)

 $q_{\rm max}$ represents the maximum cooling heat flux that the TE devices can pump from the cold side to the heatsink. Bulman *et al.* [2] reported the maximum cooling heat flux can reach 2.58×10^6 W/m².

To improve the cooling capacity of TEC, one approach is to increase the Seebeck coefficient S, electrical conductivity σ of the thermoelectric materials, such as superlattices and nanocomposites [1], [2], [27]–[29]. Another approach is to reduce the thickness L of the TEC, such as thin-film materials [1], [2], [30]. However, based on (19), thermal conductivity κ cannot change the maximum cooling heat flux value, which is unrealistic because the experiments have shown that the increasing material's figure of merit Z can improve the maximum cooling heat flux.

As a result, this model is overly simplified and gives an approximated expression to describe the Peltier, Joule heating and Fourier heat transfer effects. The results provided by the model are inaccurate when the thermal gradient is large because the formula is too simple to describe these complicated phenomena. Therefore, an accurate TEC model needs to be developed to consider spatial temperature along the TEC leg.

C. 3-D Coupled Multiphysics Model

To capture the multiphysics TE effect more accurately, the full coupled 3-D PDEs describing thermal and electric fields were introduced to analyze the TEC devices [3], [18], [21].

For the electric field, we have

$$\mathbf{E} = -\nabla \phi \tag{20}$$

where ϕ is the potential in the TEC. Then, the current continuity equation is formulated as

$$\nabla \cdot \mathbf{J} = \nabla \cdot (-\sigma \nabla \phi) = 0. \tag{21}$$

One side is set to ground boundary condition $\phi(x = 0, y, z) = 0$ and the other side is excited by an ideal voltage source $\phi(x = L, y, z) = V$.

For thermal field, we integrate the Peltier effect into the heat flux

$$\mathbf{q} = \mathbf{q}_{\text{Fourier}} + \mathbf{q}_{\text{P}} = -\kappa \nabla T + P \mathbf{J}.$$
 (22)

Then, considering the Joule heating, the heat conduction equation is rewritten as

$$\nabla \cdot \mathbf{q} = \nabla \cdot (-\kappa \nabla T + ST\mathbf{J}) = \frac{||\mathbf{J}||^2}{\sigma}.$$
 (23)

The heat sink is placed on one side to dissipate the heat, and we set this side to a constant temperature boundary condition

$$T(x = 0, y, z) = T_0$$
 (24)

where T_0 is the reference temperature (hot side for the TEC device). The other side is used to remove the heat from the chip (the cold side of the TEC device), and the boundary condition is set to the heat flux boundary condition

$$-\mathbf{n} \cdot \mathbf{q}(x = L, y, z) = -\mathbf{n} \cdot (-\kappa \nabla T + ST\mathbf{J}) = q_c \quad (25)$$

where **n** is the unit outward normal vector of the boundary surface, and q_c is the cooling heat flux. Once the cooling heat flux q_c is obtained, we can estimate the TEC devices' maximum temperature difference and maximum cooling heat flux, which are similar to Section II-B.

Several numerical methods, such as the finite-element method, finite difference method, and finite volume method, were employed to solve the coupled PDEs. Antonova and Looman [18] first performed finite-element calculation for 3-D coupled multiphysics model by using the commercial code in ANSYS. Jaegle presented an electrothermal simulation of the TEC device in the finite-element-based COMSOL Multiphysics and discretized the PDEs by using the mathematics module [21]. Yan et al. [22] and Shi et al. [23] employed the finite volume method to solve the 1-D and 2-D PDEs of TE devices, respectively. Chen et al. [24] implemented the 3-D thermoelectric generator (TEG) model in a finite volume method CFD package, which is FLUENT software. Fatch et al. [25] utilized a finite difference method to explore the design and optimization of TEG devices. However, the numerical methods require a large amount of memory and are very time-consuming for the purposes of parameter tuning and optimization of the TE devices with a large-scale N-Parray.

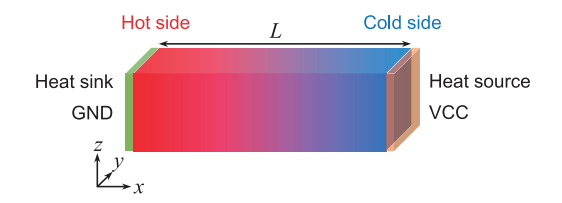


Fig. 3. Schematic of the *P*-type TEC leg. Heat source and VCC are placed on the cold side. Heat sink and GND are located on the hot side.

To mitigate the problem, an analytical solution was proposed to find the solution of the PDEs. The analytical method can provide deep insights into the physical meaning of the TEC effect. Sheikhnejad *et al.* [8] first reduced 3-D to 1-D with a realistic approximation and then used the Sturm–Liouville theorem and separation of variables method to obtain the exact solution of the PDEs. However, this work ignored the coupled effect between thermal and electric fields, and also did not obtain the maximum cooling heat flux value, which is a key performance parameter of the TEC device [1], [2], [14], [15]. Also, the analytical solution was not validated by numerical methods.

III. PROPOSED ANALYTICAL SOLUTION FOR 3-D COUPLED MULTIPHYSICS MODEL

A. Mathematical Formulation

The TEC array device analysis in Fig. 1(b) can be regarded as the superposition of multiphysics simulation of each TEC leg, as shown in Fig. 3. Because temperature and voltage change primarily along the *x*-direction, their components in *y*-direction and *z*-direction can be ignored. As a result, we can reduce the 3-D problem to 1-D one, which is consistent with the previous approach [8].

First, based on the current continuity equation and constant σ , the 1-D governing coupled equation for voltage can be expressed as

$$\nabla \cdot \mathbf{J} = \frac{\partial J}{\partial x} = \sigma \frac{\partial E}{\partial x} = 0. \tag{26}$$

The solution of (26) is given by the following general form:

$$E(x) = A \tag{27}$$

where *A* is the constant coefficient. Based on voltage boundary conditions, we have

$$\phi(L) - \phi(0) = -\int_0^L E(x)dx = -AL = V.$$
 (28)

Therefore, the constant coefficient is given by

$$A = -\frac{V}{L}. (29)$$

The current density is calculated by

$$J = \sigma E = -\sigma \frac{V}{L} \tag{30}$$

where J is along the negative direction of the x-axis (J < 0). It can be seen from (30) that the current density J is directly proportional to voltage difference V and is position-independent.

The relationship of voltage and current density is actually Ohm's law.

Second, based on (23), the 1-D heat conduction equation is written as

$$\frac{\partial}{\partial x} \left(\kappa \frac{\partial T}{\partial x} \right) - \frac{\partial (STJ)}{\partial x} + \frac{J^2}{\sigma} = 0. \tag{31}$$

We assume the thermal conductivity κ and the Seebeck coefficient S are constant. With position-independent J, (31) is rewritten as

$$\kappa \frac{\partial^2 T}{\partial x^2} - SJ \frac{\partial T}{\partial x} + \frac{J^2}{\sigma} = 0.$$
 (32)

The general solution of (32) is given by

$$T(x) = \frac{J}{S\sigma}x + C \cdot \frac{\kappa}{SJ} \exp\left(\frac{SJ}{\kappa}x\right) + D \tag{33}$$

where C and D are the coefficients. Based on thermal boundary conditions (24) and (25), we have

$$T(0) = C \cdot \frac{\kappa}{SJ} + D = T_0$$

$$\kappa \frac{\partial T}{\partial x} - STJ = \kappa \left(\frac{J}{S\sigma} + C \cdot \exp\left(\frac{SJL}{\kappa}\right) \right)$$

$$- SJ \left(\frac{J}{S\sigma} L + C \cdot \frac{\kappa}{SJ} \exp\left(\frac{SJL}{\kappa}\right) + D \right) = q_c.$$
(35)

Therefore, the coefficients are calculated by

$$C = -\frac{J}{S\sigma} + \frac{J^2L}{\kappa\sigma} + \frac{SJT_0}{\kappa} + \frac{q_c}{\kappa}$$
 (36)

$$D = \frac{\kappa}{S^2 \sigma} - \frac{JL}{S\sigma} - \frac{q_c}{SJ}.$$
 (37)

The analytical expressions (30) and (33) represent the relationship between applied voltage V, current densities J, cooling heat flux q_c , and temperature T. Based on the formulas (30) and (33), we derive the maximum temperature difference and maximum cooling heat flux of the TEC in Section IV.

Note that our proposed analytical solutions are different from the works [8] for both electric and thermal fields. For electric field, we give the current density J with respect to the voltage V and demonstrate that current density is position-independent. For thermal field, we use a more convincing heat flux boundary condition (35) which considers Peltier effect. Then, we solve heat conduction and current continuity equations in a coupled way (from $V \to J \to T$), which is different from the method (from $J \to V, J \to T$) used in [8].

B. Equivalent Thermal Circuit for 3-D Coupled Multiphysics Model

As shown in Fig. 2(a), the simplified 1-D energy equilibrium model has a corresponding equivalent thermal circuit. It turns out that we can derive an equivalent thermal circuit for 3-D coupled multiphysics model. Specifically, based on the 1-D

governing equation (32), we use finite difference method to obtain

$$\kappa \left(x + \frac{1}{2}\Delta x\right) \frac{\Delta y \Delta z}{\Delta x} (T(x + \Delta x) - T(x))$$

$$+ \kappa \left(x - \frac{1}{2}\Delta x\right) \frac{\Delta y \Delta z}{\Delta x} (T(x - \Delta x) - T(x))$$

$$- \frac{SJ\Delta y \Delta z}{2} (T(x + \Delta x) - T(x))$$

$$+ \frac{SJ\Delta y \Delta z}{2} (T(x - \Delta x) - T(x)) = -\frac{J^2}{\sigma} \Delta x \Delta y \Delta z \quad (38)$$

where Δx , Δy , and Δz are discretization lengths in x-, y-, and z-directions, respectively, $\kappa(\cdot)$ is the position-dependent thermal conductivity, and $T(\cdot)$ is a position-dependent variable. On the left-hand side of (38), the first two terms can be reviewed as the thermal conductances and the last two terms can be considered as the temperature-controlled current sources. One term on the right-hand side of (38) is the power source. Therefore, we build a new equivalent circuit for a TEC thermal cell, as shown in Fig. 2(b). The conductances and temperature-controlled current sources are represented by

$$G_{x+} = \kappa \left(x + \frac{1}{2} \Delta x \right) \frac{\Delta y \Delta z}{\Delta x}$$

$$G_{x-} = \kappa \left(x - \frac{1}{2} \Delta x \right) \frac{\Delta y \Delta z}{\Delta x}$$

$$I_{x+} = \frac{SJ \Delta y \Delta z}{2} (T(x + \Delta x, y, z) - T(x, y, z))$$

$$I_{x-} = \frac{SJ \Delta y \Delta z}{2} (T(x - \Delta x, y, z) - T(x, y, z)). \tag{39}$$

IV. OPTIMAL DESIGN OF THERMOELECTRIC COOLING

A. Maximum Temperature Difference ΔT_{max} With $q_c = 0$

Without heatload $q_c=0$, the temperature difference between the hot side and cold side is expressed as

$$\Delta T = T_h - T_c = T(0) - T(L)$$

$$= T_0 - \frac{\kappa}{S^2 \sigma} - \left(T_0 - \frac{\kappa}{S^2 \sigma} + \frac{JL}{S \sigma} \right) \exp\left(\frac{SJL}{\kappa} \right)$$

$$= \left(T_0 - \frac{1}{Z} \right) \left[1 - \exp\left(-\frac{S\sigma V}{\kappa} \right) \right] + \frac{V}{S} \exp\left(-\frac{S\sigma V}{\kappa} \right). \tag{40}$$

With voltage $V \to \infty$, the temperature difference (40) is reduced to

$$\Delta T_a = T_0 - \frac{1}{Z} \tag{41}$$

where ΔT_a is an asymptote of the curve ΔT . Fig. 4 shows the relationship between the asymptote ΔT_a and ΔT . It can be observed that there are three cases for the cooling heat flux, including $ZT_0 < 1$, $ZT_0 = 1$, and $ZT_0 > 1$. If $ZT_0 < 1$, the heat dissipation due to the Peltier and Fourier transfer effects is smaller than the heat generation caused by the Joule heating effect, and ΔT becomes negative when $V \to \infty$. If $ZT_0 = 1$, the heat removal by Peltier and Fourier transfer effects is equal to that of the Joule heating effect, and ΔT becomes 0 with $V \to \infty$. If $ZT_0 > 1$, the summation of Peltier and Fourier transfer effects is larger than the Joule heating effect, and ΔT is always positive.

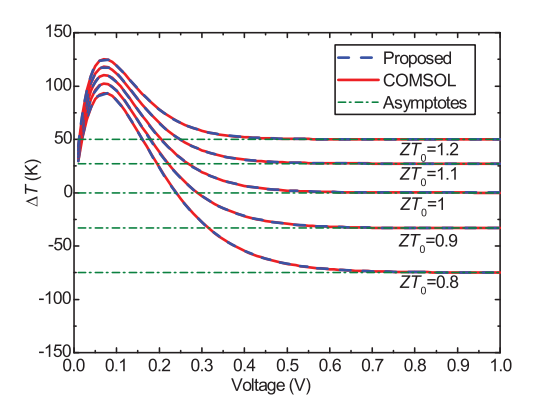


Fig. 4. Relationship between the functions ΔT and ΔT_a with different ZT_0 .

Now, we compute the optimal current density and voltage, we set the derivative of (40) is equal to 0, we have

$$J_{\text{opt},T} = -\frac{S\sigma T_0}{L}, \quad V_{\text{opt},T} = ST_0. \tag{42}$$

Therefore, the maximum temperature difference is given by

$$\Delta T_{\text{max}} = T_0 - \frac{1}{Z} [1 - \exp(-ZT_0)]. \tag{43}$$

Then, we have

$$\frac{\partial \Delta T_{\text{max}}}{\partial T_0} = 1 - \exp(-ZT_0) > 0 \tag{44}$$

$$\frac{\partial \Delta T_{\text{max}}}{\partial Z} = \frac{1}{Z^2 \exp(ZT_0)} \left[\exp(ZT_0) - (1 + ZT_0) \right]. \quad (45)$$

The Taylor series of $\exp(ZT_0)$ at 0 are expressed as

$$\exp(ZT_0) = 1 + ZT_0 + \frac{(ZT_0)^2}{2} + O((ZT_0)^3).$$
 (46)

Therefore, with (45) and (46), we obtain

$$\frac{\partial \Delta T_{\text{max}}}{\partial Z} > 0. \tag{47}$$

If we increase the material's figure of merit Z and T_0 , the maximum temperature difference will increase. However, the thickness L has no effect on the maximum temperature difference, which is consistent with (16).

B. Maximum Heat-Flux Pumping Capability q_{max} With $\Delta T = 0$

Based on (33) and $\Delta T = 0$, the cooling heat flux is expressed as

$$q_c = \left(\frac{1}{Z} - T_0\right) SJ + \frac{J^2 L}{\sigma} \frac{\exp\left(\frac{SJL}{\kappa}\right)}{1 - \exp\left(\frac{SJL}{\kappa}\right)}.$$
 (48)

We can observe that when $J \to -\infty$, the cooling heat flux becomes

$$q_{ca} = \left(\frac{1}{Z} - T_0\right) SJ. \tag{49}$$

The function q_{ca} is an asymptote of the curve q_c , as shown in Fig. 5. The green dash-dotted line is asymptote q_{ca} , and the proposed analytical solution is verified by COMOSL.

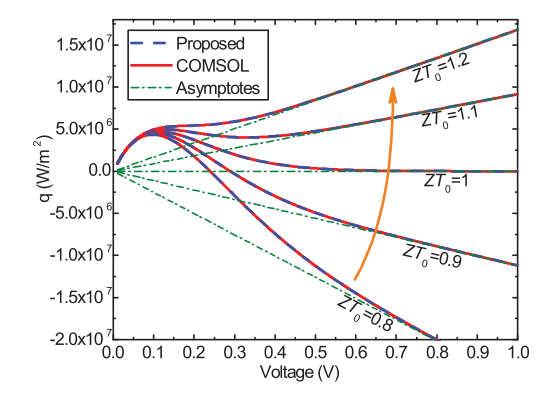


Fig. 5. Relationship between the functions q_c and q_{ca} with different ZT_0 .

C. Three Cooling Configuration Cases and Discussions

Based on the asymptote behaviors in Fig. 5, we would like to discuss three interesting cases for the cooling heat flux: $ZT_0 < 1$, $ZT_0 = 1$, and $ZT_0 > 1$ in the following.

First, in the case of $ZT_0 < 1$, there exists a maximum cooling heat flux $q_{\rm max}$. This is the case where if we keep increasing the current flow in the TEC devices, the heat generated from Joule heating will eventually be larger than the heat removed from TEC devices. As a result, we have the maximum cooling heat flux and the optimal current density.

Specifically, the derivative of q_c is given by

$$\frac{\partial q_c}{\partial J} = \left(\frac{1}{Z} - T_0\right) S + 2 \frac{JL}{\sigma} \frac{\exp\left(\frac{SJL}{\kappa}\right)}{1 - \exp\left(\frac{SJL}{\kappa}\right)} + \frac{J^2 L}{\sigma} \frac{\frac{SL}{\kappa} \exp\left(\frac{SJL}{\kappa}\right)}{\left(1 - \exp\left(\frac{SJL}{\kappa}\right)\right)^2} = 0.$$
(50)

Equation (50) is transformed into

$$a \exp^2\left(\frac{SLJ}{\kappa}\right) + b \exp\left(\frac{SLJ}{\kappa}\right) + c = 0$$
 (51)

where

$$\begin{cases} a = \left(\frac{1}{Z} - T_0\right)S - 2\frac{JL}{\sigma} \\ b = \frac{SL^2J^2}{\kappa\sigma} + 2\frac{JL}{\sigma} - 2\left(\frac{1}{Z} - T_0\right)S \\ c = \left(\frac{1}{Z} - T_0\right)S. \end{cases}$$
 (52)

Therefore, the solution of (51) is given by

$$\exp\left(\frac{SLJ}{\kappa}\right) = \frac{-b \pm \sqrt{b^2 - 4ac}}{2a}.$$
 (53)

If (53) has a real solution, we have to satisfy the condition

$$b^2 - 4ac > 0. (54)$$

The solution region of current density J is determined by

$$0 > J > J_d = 2 \frac{\sqrt{1 - ZT_0} - 1}{\frac{SL}{\kappa}}.$$
 (55)

Luck and Stevens [31] proposed an explicit solution of complex equation with the determined region of the roots. Based on the use of complex integration, the solution of (51) is calculated by the explicit expression

$$J_{\text{opt},q} = h + R \frac{\int_0^{2\pi} \omega(\theta) e^{j2\theta} d\theta}{\int_0^{2\pi} \omega(\theta) e^{j\theta} d\theta}$$
 (56)

where j denotes the imaginary number and the function $\omega(\theta)$ is defined as

$$\omega(\theta) = \frac{1}{a \exp^2\left(\frac{SLJ}{\kappa}\right) + b \exp\left(\frac{SLJ}{\kappa}\right) + c} \bigg|_{J=h+Re^{j\theta}}.$$
 (57)

The radius and center of the closed path are

$$h = (J_d - \delta)/2 + \delta, R = |(J_d - \delta)/2|$$
 (58)

where δ is a small negative value that is used to remove the point J = 0.

Second, if $ZT_0 = 1$, there is also a maximum cooling heat flux q_{max} . This case is similar to the case of $ZT_0 < 1$ except that the heat generation from Joule heating and heat removal from TEC reach the same level, which means increasing current density or voltage of TEC devices will lead to zero cooling heat flux, as shown in Fig. 5.

Specifically, the derivative $[\partial q_c/\partial J]$ becomes

$$\frac{\partial q_c}{\partial J} = 2 \frac{JL}{\sigma} \frac{\exp\left(\frac{SJL}{\kappa}\right)}{1 - \exp\left(\frac{SJL}{\kappa}\right)} + \frac{J^2L}{\sigma} \frac{\frac{SL}{\kappa} \exp\left(\frac{SJL}{\kappa}\right)}{\left(1 - \exp\left(\frac{SJL}{\kappa}\right)\right)^2} = 0. (59)$$

Therefore, we obtain the optimal current density

$$J_{\text{opt},q} = -\frac{\kappa}{LS} \left(2 + W \left(-\frac{2}{e^2} \right) \right) \tag{60}$$

where $W(\cdot)$ is a Lambert function. The corresponding maximum cooling heat flux is given by

$$q_{\text{max}} = \left(2 + W\left(-\frac{2}{e^2}\right)\right)^2 \frac{\kappa^2}{LS^2\sigma} \frac{\exp\left(-\left(2 + W\left(-\frac{2}{e^2}\right)\right)\right)}{1 - \exp\left(-\left(2 + W\left(-\frac{2}{e^2}\right)\right)\right)}.$$
(61)

Third, when $ZT_0 > 1$, this is the case that the cooling capacity of TEC devices due to Peltier and Fourier transfer effects is larger than the heat generation caused by the Joule heating effect. As a result, there is no global maximum cooling heat flux. As we can see that the cooling heat flux increases with the increasing current density J, as shown in Fig. 5. To the best of our knowledge, this new phenomenon is first observed by the new analytical formula of the cooling heat flux. In this case, we can simply increase the TEC current density to reduce any excessive on-chip and hot spot temperatures as we want. But practically, we will see that we cannot simply increase current or voltage as the power/energy efficiency will diminish very quickly and there are also many reliability issues with high current and voltages as shown in the following section.

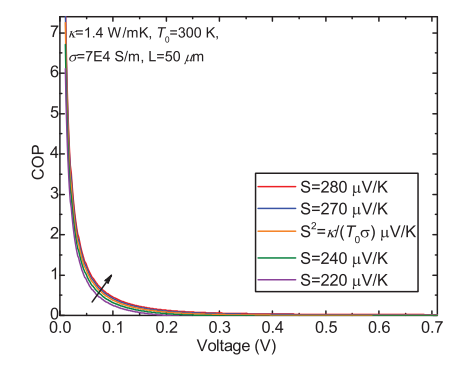


Fig. 6. COP of a TEC leg with different Seebeck coefficients.

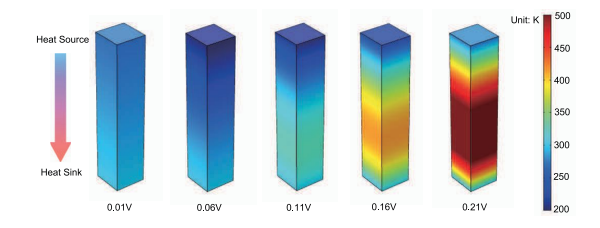


Fig. 7. Temperature profiles of the TEC leg with $q_{\rm c}=0$ and different voltages between the two terminals.

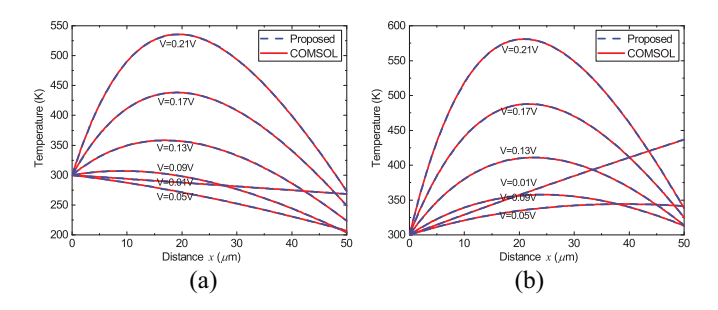


Fig. 8. Temperature distributions of the TEC leg calculated by COMSOL and the proposed method for cooling heat flux (a) $q_c=0$ and (b) $q_c=5\times 10^6~\rm W/m^2$.

D. Limitation and Assumption Discussion

As with any work, the proposed method depends on some assumptions and has also some limitations as well. First, to obtain an analytical solution for 3-D coupled multiphysics model, we assume that S, σ , and κ are constant, which can lead to the error because temperature has an impact on these parameters. This analytical solution also does not consider the electrical and thermal contact resistances, which can degrade the cooling performance of the TEC devices [2]. The temperature boundary condition that we use to represent heat sink is ideal because a real heat sink has limited cooling capacity and cannot keep temperature constant on the hot side. These limitations will be addressed in future work.

Figs. 9–11 show that TEC devices have extremely high cooling performance. This is because we modify the parameters $(S, \sigma, \text{ and } \kappa)$ to achieve $ZT_0 > 1$ and study the phenomenon that cooling heat flux can be improved infinitely with increasing voltage. We also want to use these results to validate the accuracy of the proposed analytical solution by comparison with COMSOL. Several articles have reported that BiTe-based materials can achieve ZT > 1 [1], [2], [32].

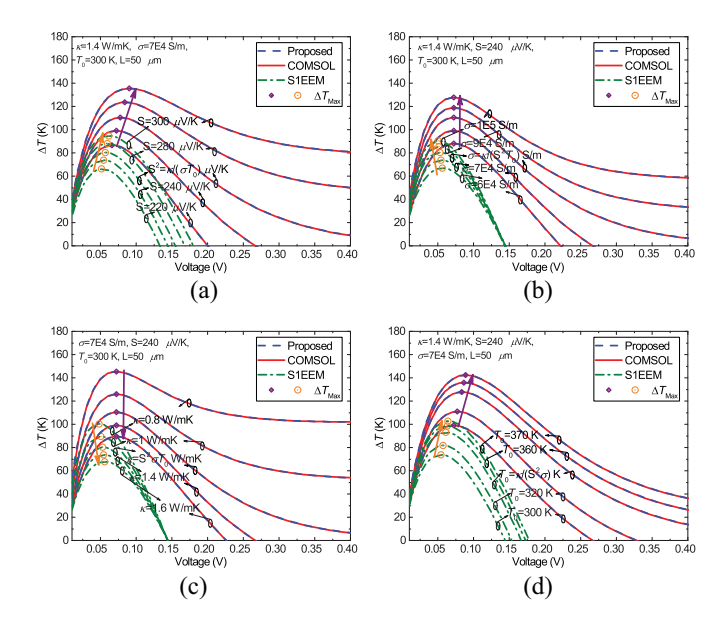


Fig. 9. Temperature difference ΔT versus voltage V of the TEC leg with different (a) Seebeck coefficient S, (b) electrical conductivity σ , (c) thermal conductivity κ , and (d) heat sink temperature T_0 . The purple diamond and orange circle represent maximum temperature difference $\Delta T_{\rm max}$ for the proposed method and S1EEM, respectively.

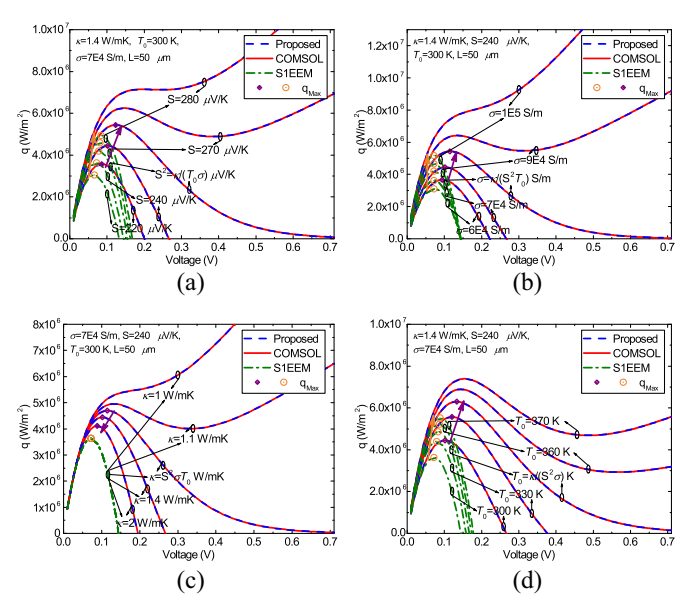


Fig. 10. Cooling heat flux q_c versus voltage V of the TEC leg with different (a) Seebeck coefficient S, (b) electrical conductivity σ , (c) thermal conductivity κ , and (d) heat sink temperature T_0 . The purple diamond and orange circle represent maximum cooling heat flux $q_{\rm max}$ for the proposed method and S1EEM, respectively.

However, S, σ , and κ are temperature-dependent so that ZT is also temperature-dependent. The maximum ZT can be larger than 1. But, it is difficult to keep ZT > 1 over the whole temperature range. Although the range of these parameters we used is similar to the range of $Bi_{0.5}Sb_{1.5-x}M_xTe_3$ (M = Cd, Cu, and Ag) materials' properties [32], their combination may not exist in real world. Because there are mutual dependencies of S, σ , and κ . For example, when S is increased, σ decreases and κ becomes large. As a result, ZT is reduced. In practice, we cannot easily modify these parameters to the values as we

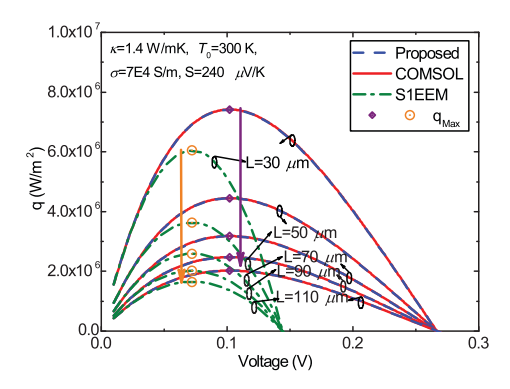


Fig. 11. Cooling heat flux q_c versus voltage V of the TEC leg with different thickness L.

like. In addition, ZT_0 we defined is different from ZT. When $T > T_0$, we have $ZT > ZT_0$. Therefore, ZT > 1 does not mean $ZT_0 > 1$. In summary, it is not easy to satisfy the condition $ZT_0 > 1$ for real TE materials.

Theoretically, we can increase the cooling heat flux without an upper bound by increasing the voltage. However, there are several factors, which may limit such simple operation to increase cooling flux from TEC devices. One is thermal reliability. When the voltage is increased, the temperature in the middle of the TEC leg can become significant, as shown in Fig. 8. High temperature degrades not only the cooling performance but also the thermal reliability of the TEC devices. The other is energy conversion efficiency, which is evaluated by coefficient of performance (COP) defined as [16]

$$COP = \frac{\text{heat absorbed}}{\text{electrical power input}} = \frac{|q_c A|}{|VI|} = \frac{q_c}{-JV}$$

$$= \frac{\left(\frac{1}{Z} - T_0\right)SJ + \frac{J^2L}{\sigma} \frac{\exp\left(\frac{SJL}{\kappa}\right)}{1 - \exp\left(\frac{SJL}{\kappa}\right)}}{J^2L/\sigma}$$

$$= \left(T_0 - \frac{1}{Z}\right)\frac{S}{V} + \frac{\exp\left(-\frac{S\sigma V}{\kappa}\right)}{1 - \exp\left(-\frac{S\sigma V}{\kappa}\right)}.$$
(62)

The larger COP, the higher energy conversion efficiency. As shown in Fig. 6, the COP will diminish with the increasing voltage, which means the cooling heat flux cannot be improved significantly even when voltage is increased a lot and the majority of electrical power is wasted. This method is not economic in real applications.

V. NUMERICAL RESULTS AND DISCUSSION

The TEC leg, as shown in Fig. 3, is employed to validate our proposed analytical solution and optimization formula for the 3-D coupled multiphysics model. First, the accuracy of the analytical solution is verified by finite-element-based COMSOL Multiphysics [33] in Section V-A. Then, the impacts of parameters, such as Seebeck coefficient S, thermal conductivity κ , electrical conductivity σ , heat sink temperature T_0 , and the thickness L, on maximum temperature difference $\Delta T_{\rm max}$ and maximum cooling heat flux $q_{\rm max}$ are presented in Sections V-B and V-C, respectively. Last, we give

a comparison between the proposed analytical solution and the simplified 1-D energy equilibrium model in Section V-D.

BiTe-based compounds are still promising TE materials and widely used in TE cooling applications. The electrical and thermal properties of TE materials are temperature-dependent. Hao *et al.* [32] obtained temperature-dependent S, σ , and κ for Bi $_{0.5}{\rm Sb}_{1.5-x}{\rm M}_x{\rm Te}_3$ (M = Cd, Cu, and Ag) samples in the temperature range of 300–600K. S ranges from 120 to 240 $\mu{\rm V/K}$. σ is around 2 × 10⁴-1.8 × 10⁵ S/m. κ varies in the range of 0.8–1.4 W/(mK). ZT is from 0.2 to 1.4. Therefore, we set the Seebeck coefficient S = 240 $\mu{\rm V/K}$, electrical conductivity σ = 7 × 10⁴ S/m, and thermal conductivity κ = 1.4 W/(mK) as basic values (ZT_0 < 1).

To demonstrate the three cases ($ZT_0 < 1$, $ZT_0 = 1$, and $ZT_0 > 1$), we modify the values of S, σ , and κ based on the basic values. The parameters S of 220–300 μ V/K, σ of 6– 10×10^4 S/m, and κ of 0.8–1.6 W/(mK) are employed to observe the new phenomenon that there is no upper bound for the cooling heat flux when $ZT_0 > 1$, which may not exist in the real world.

A. Accuracy of the Analytical Expression for 3-D Coupled Multiphysics Model

Fig. 3 shows a 3-D structure of the TEC leg with dimension $10 \ \mu m \times 10 \ \mu m \times 50 \ \mu m$. The thermal boundary conditions are temperature boundary $T_0 = 300$ K and heat flux boundary q_c . The electrical boundary conditions are voltage $\phi(0) = 0$ V and $\phi(L) = V$.

First, we use the COMSOL Mathematics module to implement the 3-D coupled multiphysics model. Fig. 7 shows the temperature profiles calculated by COMSOL of TEC leg with $q_c=0$ and different voltages. When the voltage is increased, cooling heat due to Peltier effect is improved. If we continue to increase the voltage, Joule heating effect, which degrades the cooling performance of the TEC leg, becomes serious. Therefore, voltage has an optimal value to reach the maximum cooling performance of the TEC.

Second, our proposed analytical method is employed to perform electrothermal simulation of the TEC leg. The temperature distributions from the proposed method and COMSOL are shown in Fig. 8. They agree well with each other. It demonstrates that the approximation from 3-D to 1-D has a negligible loss and the proposed method is very accurate. Fig. 8(a) and (b) shows temperature distributions of TEC leg with and without workload, respectively. It can be observed that the temperature of cold side will increase dramatically when workload $q_c = 5 \times 10^6 \text{ W/m}^2$ is added. The workload q_c , called cooling heat flux, is a key parameter for the cooling performance of TEC.

B. Maximum Temperature Difference ΔT_{max} With $q_c = 0$ and Different Parameters

In order to study the cooling performance, the relationship between temperature difference ΔT and voltage V without workload using the proposed method and S1EEM is illustrated in Fig. 9. The legend "S1EEM" denotes a simplified 1-D energy equilibrium model. It can be observed from Fig. 9

that there exists the maximum temperature difference $\Delta T_{\rm max}$, which is proportional to ZT_0 by using both proposed method and S1EEM. It should be noted that both proposed method and S1EEM demonstrate the thickness L of TEC leg has no effect on $\Delta T_{\rm max}$. We also observe that when the value of temperature difference ΔT is maximum, the cooling heat flux q_c does not reach the maximum value, which is described in Section V-C.

C. Maximum Heat-Flux Pumping Capability q_{max} With $\Delta T = 0$ and Different Parameters

For further assessment of the cooling performance, the impact of ZT_0 on the cooling heat flux q_c is shown in Fig. 10. It can be observed from Fig. 10 that when $ZT_0 \leq 1$, there exists the maximum cooling heat flux $q_{\rm max}$, which is proportional to ZT_0 by using the proposed method. However, S1EEM fails to predict the thermal conductivity κ impact on the cooling heat flux, as shown in Fig. 10(c). Note that there is no $q_{\rm max}$ in the case of $ZT_0 > 1$, as shown in Fig. 10. As we can see, the cooling heat flux continues to increase when the applied voltage becomes larger. This is because the heat dissipation due to Peltier and Fourier transfer effects is larger than the heat generated by Joule heating effect, which provides an alternative way to improve the cooling performance.

Fig. 11 shows smaller thickness L can lead to larger $q_{\rm max}$ by using both the proposed method and S1EEM. The optimal voltage is located at the region of 0.1–0.2 V, which only depends on ZT_0 and is the independence of thickness L. However, the optimal current density depends on both ZT_0 and L. In the case of $L=50~\mu{\rm m}$ and $\sigma=7\times10^4~{\rm S/m}$, the optimal current density ranges from 1.4×10^8 to $2.8\times10^8~{\rm A/m}^2$.

Based on Figs. 10 and 11, there are two approaches to improve the cooling performance of the TEC device [2]. One is to develop thermoelectric materials with a high ZT_0 . That is to say, S, σ , and T_0 should be large and κ should be small [32]. Another is to reduce the thickness of thermoelectric materials [1], such as ultrathin nanostructured Bi₂Te₃-based superlattices. The maximum cooling heat flux for the bulk-based TE materials is approximately 1×10^5 W/m² [14]. The commercial thin-film TEC devices with 20 μ m thick have a maximum cooling heat flux of $1 \times 10^6 \text{W/m}^2$ [15]. Recently, the TEC devices with 8 µm Bi₂Te₃-based thin-film superlattice materials can achieve 2.58×10^6 W/m² [2]. However, our results show the maximum heat flux is $\sim 7.5 \times 10^6$ W/m², which is higher than the performance of real TEC devices because of the limitation illustrated in Section IV-D. For the silicon microprocessors, the average heat flux is up to 1×10^7 W/m² and is extremely high at localized hotspots [34], which is an order of magnitude higher than that of the latest TEC cooler. Therefore, the performance of current TEC devices still needs to be improved to meet on-demand cooling in electronic devices.

To demonstrate the efficiency of the proposed analytical solution by comparison with finite-element-based COMSOL, Fig. 10(a) is taken as an example to calculate the cooling heat flux q_c of the TEC leg with temperature difference $\Delta T=0$, voltage V of 0–0.7 V ($\Delta V=0.001$ V) and Seebeck coefficient S of 220–280 μ V/K. In COMSOL, the mesh element

TABLE I EFFICIENCY AND MEMORY COMPARISON

	Time	Memory
Analytic	~0.01 s	∼1 MB
COMSOL	3026 s	2.64 GB

size is set as normal and the number of degrees of freedom is 2445. The proposed analytical method is implemented using MATLAB. The computational time and used memory are listed in Table I. Therefore, the proposed analytical method has a great advantage over COMSOL in both time and memory usage.

D. Comparison of the Proposed Analytical Solution and S1EEM

It can be observed from Figs. 9–11 that the results from the proposed method and S1EEM have a good agreement at small voltage. However, the discrepancy between the proposed method and S1EEM becomes large with the increasing voltage. The simple approximation of S1EEM is only suitable for small voltage and little TEC effect. When the Peltier, Joule heating, and Fourier transfer effects become more serious due to the higher voltage, the coupled PDEs should be employed to describe the thermal and electric fields. In addition, S1EEM cannot predict the thermal conductivity κ impact on the cooling heat flux. Therefore, the analytical coupled multiphysics model is a more robust and accurate model for the TEC device compared to S1EEM.

VI. CONCLUSION

In this article, we have proposed an analytical approach for multiphysics electrothermal simulation of thermoelectric cooling. Based on the resulting analytic expressions for temperature, the maximum temperature difference and cooling heat flux are derived to guide the design of thermoelectric cooler to achieve the maximum cooling performance. Furthermore, we observed, for the first time, that when the ZT_0 value is larger than 1, the cooling heat flux continues to increase with increasing voltage, which means the heat dissipation due to the Peltier and Fourier transfer effects is larger than the heat generation caused by Joule heating effect. The accuracy of the proposed formulas is verified using the finite-element-based COMSOL software. The compact model delivers many orders of magnitude speedup and memory saving compared to COMSOL with marginal accuracy loss. Compared with the conventional simplified 1-D energy equilibrium model, the proposed analytical coupled multiphysics model is more robust and accurate.

REFERENCES

- I. Chowdhury et al., "On-chip cooling by superlattice-based thinfilm thermoelectrics," Nat. Nanotechnol., vol. 4, no. 4, pp. 235–238, Jan. 2009.
- [2] G. Bulman *et al.*, "Superlattice-based thin-film thermoelectric modules with high cooling fluxes," *Nat. Commun.*, vol. 7, no. 1, pp. 1–13, Ian 2016

- [3] R. A. Kishore, A. Nozariasbmarz, B. Poudel, M. Sanghadasa, and S. Priya, "Ultra-high performance wearable thermoelectric coolers with less materials," *Nat. Commun.*, vol. 10, no. 1, pp. 1–13, Apr. 2019.
- [4] F. Kaplan, M. Said, S. Reda, and A. K. Coskun, "LoCool: Fighting hot spots locally for improving system energy efficiency," *IEEE Trans. Comput.-Aided Design Integr. Circuits Syst.*, vol. 39, no. 4, pp. 895–908, Apr. 2020.
- [5] J. Long and S. O. Memik, "A framework for optimizing thermoelectric active cooling systems," in *Proc. Design Autom. Conf.*, 2010, pp. 591–596.
- [6] J. Long, S. O. Memik, and M. Grayson, "Optimization of an on-chip active cooling system based on thin-film thermoelectric coolers," in *Proc. Design Autom. Test Eur.*, 2010, pp. 117–122.
- [7] J. Long, D. Li, S. O. Memik, and S. Ulgen, "Theory and analysis for optimization of on-chip thermoelectric cooling systems," *IEEE Trans. Comput.-Aided Design Integr. Circuits Syst.*, vol. 32, no. 10, pp. 1628–1632, Oct. 2013.
- [8] Y. Sheikhnejad, R. Bastos, Z. Vujicic, A. Shahpari, and A. Teixeira, "Laser thermal tuning by transient analytical analysis of peltier device," *IEEE Photon. J.*, vol. 9, no. 3, pp. 1–13, Jun. 2017.
- [9] M. P. Gupta, M.-H. Sayer, S. Mukhopadhyay, and S. Kumar, "Ultrathin thermoelectric devices for on-chip peltier cooling," *IEEE Trans. Compon. Packag. Manuf. Technol.*, vol. 1, no. 9, pp. 1395–1405, Sep. 2011.
- [10] P. Wang, P. McCluskey, and A. Bar-Cohen, "Hybrid solid- and liquid-cooling solution for isothermalization of insulated gate bipolar transistor power electronic devices," *IEEE Trans. Compon. Packag. Manuf. Technol.*, vol. 3, no. 4, pp. 601–611, Apr. 2013.
- [11] L. A. Nimmagadda and S. Sinha, "Thermoelectric property requirements for on-chip cooling of device transients," *IEEE Trans. Electron Devices*, vol. 67, no. 9, pp. 3716–3721, Sep. 2020.
- [12] X.-L. Shi, J. Zou, and Z.-G. Chen, "Advanced thermoelectric design: From materials and structures to devices," *Chem. Rev.*, vol. 120, no. 15, pp. 7399–7515, 2020.
- [13] K. Xie and M. C. Gupta, "High-temperature thermoelectric energy conversion devices using Si-Ge thick films prepared by laser sintering of nano/micro particles," *IEEE Trans. Electron Devices*, vol. 67, no. 5, pp. 2113–2119, May 2020.
- [14] G. E. Bulman, E. Siivola, R. Wiitala, R. Venkatasubramanian, M. Acree, and N. Ritz, Three-stage thin-film superlattice thermoelectric multistage microcoolers with a ΔT_{max} of 102 K," *J. Electron. Mater.*, vol. 38, no. 7, pp. 1510–1515, 2009.
- [15] B. Habbe and J. Nurnus, "Thin film thermoelectrics today and tomorrow," *Electron. Cooling*, vol. 17, pp. 24–31, Sep. 2011.
- [16] D. M. Rowe, Thermoelectrics Handbook: Macro to Nano. Boca Raton, FL, USA: CRC Press, 2005.
- [17] L. Chen, R. Liu, and X. Shi, Thermoelectric Materials and Devices. Cambridge, MA, USA: Elsevier, 2020.
- [18] E. E. Antonova and D. C. Looman, "Finite elements for thermoelectric device analysis in ANSYS," in *Proc. 24th Int. Conf. Thermoelectr. (ICT)*, 2005, pp. 215–218.
- [19] C. Goupil, Continuum Theory and Modeling of Thermoelectric Elements. Weinheim, Germany: Wiley-VCH, 2015.
- [20] T.-H. Wang, Q.-H. Wang, C. Leng, and X.-D. Wang, "Parameter analysis and optimal design for two-stage thermoelectric cooler," *Appl. Energy*, vol. 154, pp. 1–12, Sep. 2015.
- [21] M. Jaegle, "Multiphysics simulation of thermoelectric system— Modeling of peltier cooling and thermoelectric generator," in *Proc. COMSOL Conf.*, 2008, pp. 4–6.
- [22] D. Yan, F. P. Dawson, M. Pugh, and A. A. El-Deib, "Time-dependent finite-volume model of thermoelectric devices," *IEEE Trans. Ind. Appl.*, vol. 50, no. 1, pp. 600–608, Jan./Feb. 2014.
- [23] Y. Shi, Y. Wang, D. Mei, and Z. Chen, "Numerical modeling of the performance of thermoelectric module with polydimethylsiloxane encapsulation," *Int. J. Energy Res.*, vol. 42, no. 3, pp. 1287–1297, 2018.
- [24] M. Chen, L. Rosendahl, and T. Condra, "A three-dimensional numerical model of thermoelectric generators in fluid power systems," *Int. J. Heat Mass Transf.*, vol. 54, nos. 1–3, pp. 345–355, 2011.
- [25] H. Fateh, C. A. Baker, M. J. Hall, and L. Shi, "High fidelity finite difference model for exploring multi-parameter thermoelectric generator design space," *Appl. Energy*, vol. 129, pp. 373–383, Sep. 2014.
- [26] S. H. Choday, K. Kwon, and K. Roy, "Workload dependent evaluation of thin-film thermoelectric devices for on-chip cooling and energy harvesting," in *Proc. IEEE/ACM Int. Conf. Comput.-Aided Design*, 2014, pp. 535–541.

- [27] A. Shakouri, "Nanoscale thermal transport and microrefrigerators on a chip," *Proc. IEEE*, vol. 94, no. 8, pp. 1613–1638, Aug. 2006.
- [28] S. I. Kim *et al.*, "Dense dislocation arrays embedded in grain boundaries for high-performance bulk thermoelectrics," *Science*, vol. 348, no. 6230, pp. 109–114, 2015.
- [29] B. Poudel *et al.*, "High-thermoelectric performance of nanostructured bismuth antimony telluride bulk alloys," *Science*, vol. 320, no. 5876, pp. 634–638, 2008.
- [30] R. Venkatasubramanian, E. Siivola, T. Colpitts, and B. O'Quinn, "Thin-film thermoelectric devices with high room temperature figures of merit," *Nature*, vol. 413, no. 6856, pp. 597–602, Oct. 2001.
- [31] R. Luck and J. W. Stevens, "Explicit solutions for transcendental equations," SIAM Rev., vol. 44, no. 2, pp. 227–233, 2002.
- [32] F. Hao et al., "High efficiency Bi₂Te₃-based materials and devices for thermoelectric power generation between 100 and 300° C," Energy Environ. Sci., vol. 9, no. 10, pp. 3120–3127, 2016.
- [33] COMSOL Multiphysics User's Guide, COMSOL Multiphys., Burlington, MA, USA, Sep. 2016.
- [34] J. W. Palko et al., "Extreme two-phase cooling from laser-etched diamond and conformal, template-fabricated microporous copper," Adv. Funct. Mater., vol. 27, no. 45, 2017, Art. no. 1703265.



Liang Chen (Member, IEEE) was born in 1992. He received the B.E. degree in electromagnetic field and wireless technology from Northwestern Polytechnical University, Xi'an, China, in 2015, and the Ph.D. degree in electronic science and technology from Shanghai Jiao Tong University, Shanghai, China, in 2020.

He is currently a Postdoctoral Researcher with the VLSI System and Computation Laboratory, Department of Electrical and Computer Engineering, University of California at Riverside, Riverside, CA,

USA. His current research interests include signal integrity of high-speed interconnects, electrothermal co-simulation of 3-D integrated packages, and electromigration reliability.



Sheriff Sadiqbatcha (Graduate Student Member, IEEE) received the B.S. degree (most outstanding graduate of the year) in computer engineering from California State University, Bakersfield, CA, USA, in 2016, and the M.S. degree (magna cum laude) in electrical engineering from the University of California at Riverside, Riverside, CA, USA, in 2019, where he is currently pursuing the Ph.D. degree with the Department of Electrical and Computer Engineering.

His research interests include pre-silicon reliabil-

ity (electromigration), and applied machine-learning in the area of electronic design automation, post-silicon thermal, power, and reliability modeling and control



Hussam Amrouch (Member, IEEE) received the Ph.D. degree (*summa cum laude*, with Distinction) from Karlsruhe Institute of Technology (KIT), Karlsruhe, Germany, in 2015.

He is a Junior Professor of the Semiconductor Test and Reliability (STAR) Chair, Computer Science, Electrical Engineering Faculty, University of Stuttgart, Stuttgart, Germany, and a Research Group Leader with KIT, Karlsruhe, Germany. He has 115 publications (including 43 journals) in multidisciplinary research areas across the entire computing

stack, starting from semiconductor physics to circuit design all the way up to computer-aided design and computer architecture. His main research interests are design for reliability and testing from device physics to systems, machine learning, security, approximate computing, and emerging technologies with a special focus on ferroelectric devices.

Dr. Amrouch holds seven HiPEAC Paper Awards and three best paper nominations at top EDA conferences: DAC'16, DAC'17, and DATE'17 for his work on reliability. He currently serves as an Associate Editor of *Integration, the VLSI Journal*. He has served in the technical program committees of many major EDA conferences, such as DAC, ASP-DAC, and ICCAD, and as a Reviewer in many top journals, such as IEEE TRANSACTIONS ON ELECTRON DEVICES, IEEE TRANSACTIONS ON CIRCUITS AND SYSTEMS—PART I: REGULAR PAPERS, IEEE TRANSACTIONS ON VERY LARGE SCALE INTEGRATION SYSTEMS (VLSI), IEEE TRANSACTIONS ON COMPUTER-AIDED DESIGN OF INTEGRATED CIRCUITS AND SYSTEMS, and IEEE TRANSACTIONS ON COMPUTERS.



Sheldon X.-D. Tan (Senior Member, IEEE) received the B.S. and M.S. degrees in electrical engineering from Fudan University, Shanghai, China, in 1992 and 1995, respectively, and the Ph.D. degree in electrical and computer engineering from the University of Iowa, Iowa City, IA, USA, in 1999.

He is a Professor with the Department of Electrical Engineering, University of California at Riverside, Riverside, CA, USA, where he also is a Cooperative Faculty Member with the Department of Computer Science and Engineering. He was a

Visiting Professor with Kyoto University, Kyoto, Japan, as a JSPS Fellow from December 2017 to January 2018. His research interests include machine and deep learning for VLSI reliability modeling and optimization at circuit and system levels, machine learning for circuit and thermal simulation, thermal modeling, optimization and dynamic thermal management for many-core processors, efficient hardware for machine learning and AI, parallel computing and simulation based on GPU and multicore systems. He has published more than 320 technical papers and has coauthored six books on those areas.

Prof. Tan received the NSF CAREER Award in 2004, the Best Paper Awards from ICSICT'18, ASICON'17, ICCD'07, and DAC'09. He also received the Honorable Mention Best Paper Award from SMACD'18. He is serving as the TPC Chair for ASPDAC 2021, and the TPC Vice Chair for ASPDAC 2020. He is serving or served as the Editor in Chief for Integration, the VLSI Journal (Elsevier), an Associate Editor for four journals: IEEE TRANSACTIONS ON VERY LARGE SCALE INTEGRATION SYSTEMS (VLSI), ACM Transactions on Design Automation of Electronic Systems, Microelectronics Reliability (Elsevier), and Electronics Microelectronics and Optoelectronics Section (MDPI).